Journal of Hydrology 513 (2014) 467–474

Contents lists available at ScienceDirect

Journal of Hydrology

journal homepage: www.elsevier.com/locate/jhydrol

Nowcasting of rain events using multi-frequency radiometric observations

Rohit Chakraborty, Saurabh Das, Soumyajyoti Jana, Animesh Maitra *

S.K. Mitra Centre for Research in Space Environment, Institute of Radio Physics and Electronics, University of Calcutta, Kolkata, India

ARTICLE INFO

Article history:
Received 20 August 2013
Received in revised form 24 March 2014
Accepted 28 March 2014
Available online 13 April 2014
This manuscript was handled by A. Bardossy, Editor-in-Chief, with the assistance of Attilio Castellarin, Associate Editor

Keywords:
Nowcasting
Multi-frequency radiometer
Brightness temperature
Water vapor
Tropical rain

SUMMARY

Nowcasting of heavy rain events using microwave radiometer has been carried out at Kolkata (22.65°N, 88.45°E), a tropical location. Microwave radiometer can produce the temperature and humidity profiles of the atmosphere with fairly good accuracy. Definite changes are observed in temperature and humidity profiles before and at the onset of heavy rain events. Concurrent changes in the brightness temperatures (BT) at 22 GHz and 58 GHz are found to be suitable to nowcast rain. The time derivatives of brightness temperatures at 22 GHz and 58 GHz are used as inputs to the proposed nowcasting model. In addition, the standard deviation of the product of these time derivatives is also considered. The model has been developed using the data of 2011 and validated for rain events of 2012–2013 showing a prediction efficiency of about 90% with alarm generated about 25 min in advance.

1. Introduction

In the Indian subcontinent, sudden and heavy precipitations occur during pre monsoon period of March–May and monsoon period of June–September. These forms of precipitations are found to affect agriculture, aviation and in severe cases can cause loss of life and property. Nowcasting of heavy precipitations has many applications in mitigating some of the adverse situations resulting from such events.

Conventionally, satellite and radar data are used to nowcast thunderstorms (Browning, 1982; Cluckie and Collier, 1991; Dutta et al., 2010; Mecklenburg et al., 2000; Sokol, 2006; Wang et al., 2009; Wilson et al., 1998; Zahraei et al., 2013). The reported prediction efficiencies are usually around 80% with false alarm rates above 25% for both radar and numerical weather prediction (NWP) based nowcasting (Johnson and Olsen, 1998; Wilson et al., 1998; Lin et al., 2005). The temperature and humidity profiles of the atmosphere along with the instability indices obtained from atmospheric sounding measurements such as radiosondes can also be a useful tool for rain and thunderstorm predictions (Geerts, 2001; Manzato, 2003; McCann, 1994). Except radar, these instruments suffer from poor temporal resolution. However radars are costly and need much involved maintenance for continuous operation.

Heavy rain events also create attenuation of microwave signals. So microwave propagation through the atmosphere can provide a useful signature of heavy rain events. In this connection atmospheric brightness temperatures measured by a microwave radiometer can be useful for nowcasting of rain (Koffi et al., 2007; Won et al., 2009). Güldner and Spänkuch (1999) showed that the liquid water content (LWC) and perceptible water vapor (PWV) increases before rain. So an increase of brightness temperature (BT) in water vapor channels (22–31 GHz) can be observed about 2 h before rain (Won et al., 2009). Many convective indices from radiometer have been utilized for nowcasting heavy precipitation events (Darkow, 1968; Faubush et al., 1951; Galway, 1956; Madhulatha et al., 2013; Showalter, 1953). There are some efforts to predict rain using a microwave radiometer. Dvorak et al. (2012) used BT at 10 GHz to predict rain with a hit ratio of 74% and a false alarm rate of 7%. Won et al. (2009) also used BT at 22, 30 and 51 GHz for rain prediction with a probability of detection 0.9 for rain accumulated below 20 mm.

* Corresponding author. Address: Institute of Radio Physics and Electronics, University of Calcutta, 92, Acharya Prafulla Chandra Road, Kolkata 700009, India. Tel.: +91 33 2350 9116x28 (Office); fax: +91 33 2351 5828.

E-mail addresses: rohitc744@gmail.com (R. Chakraborty), das.saurabh01@gmail.com (S. Das), mantu.abc@gmail.com (S. Jana), animesh.maitra@gmail.com, am.rpe@caluniv.ac.in (A. Maitra).

http://dx.doi.org/10.1016/j.jhydrol.2014.03.066
0022-1694/

However, models using radiometric observations are not highly accurate for nowcasting rain (Chan and Lee, 2011; Wilson et al., 1998; Won et al., 2009). The primary reason could be that an increase of atmospheric water vapor has been taken to be the only precursor of intense convective activities. However, water vapor can also increase significantly in the absence of rain (Sherwood et al., 2010; Won et al., 2009). So monitoring of other parameters of the atmosphere is also needed.

The radio environment over Kolkata (22.65°N, 88.45°E) has been studied using a multi-frequency profiler radiometer. Since convective rain is usually associated with drastic change in water vapor as well as temperature, brightness temperatures of water vapor and oxygen absorption bands can be considered to be indicators of the impending rain events.

2. Experimental setup and data

A Dicke radiometer system (RPG-HATRO) is used for the present study. It consists of two receiving sections along with a noise diode, a data acquisition system, rain sensor, GPS clock, and a ground pressure and temperature sensor (Rose and Czekala, 2009). It measures the brightness temperatures in the range of 0–800 K with an accuracy of 0.5 K at 14 frequencies in two frequency bands (7 frequencies in each band). As the first frequency band (22–31.4 GHz) is sensitive to water vapor absorption, it is used for humidity profiling. The frequency band (51.26–58 GHz), being sensitive to oxygen absorption, is utilized to obtain the temperature profile of the troposphere. A quadratic regression retrieval algorithms are employed to convert the brightness temperatures into atmospheric parameters like temperature profile, humidity profile, integrated water vapor (IWV) and liquid water content (LWC).

The radiometric system employs three types of calibration. In absolute calibration, a linear calibration curve between receiver voltage and antenna temperature is obtained by exposing the receiver to two different sources, an ambient target and liquid nitrogen target of 77 K. Since absolute calibration cannot be imparted frequently, the noise injection calibration is implemented, every 25–30 min, by using a noise diode which acts as a standard noise source. The radiometer is further calibrated once in every cycle to filter out cosmic and path length noises in the 22–31 GHz band by measuring the brightness temperatures at various elevation angles. This technique is known as the sky-tipping calibration.The relation between the profiles of atmospheric parameters and brightness temperatures (BT) are obtained using radiative transfer theory. About 15,000 radiosonde profiles of Kolkata have been utilized to obtain the retrieval algorithm. Quadratic regression inversion technique has been used to convert the brightness temperature to temperature and humidity profiles.

An impact type disdrometer (RD-80, Waldgovel type) is also used for ground based rain rate measurements for the present study.

Brightness temperature data from radiometer and rain rate data from disdrometer are collected for the year of 2011. From the dataset, 44 days where rain event occurred during pre-monsoon (March–May) and monsoon (June–September) period of 2011 have been utilized to develop the model for rain prediction. The rain events of at least 5 min duration and having the maximum rain rate exceeding 10 mm/h are considered for the study. To validate the efficacy of the model, it is tested on a new dataset comprising 130 rainy days of premonsoon and monsoon period of 2012 (March 2012–September 2012) and premonsoon period of 2013 (March 2013–June 2013).

To have a quality check of the data, the retrieved temperature and relative humidity profiles obtained with radiometer are compared with radiosonde measurements during the years 2011–2012 obtained by India Meteorological Department, Kolkata (<10 km aerial distance). A correlation coefficient value of 0.94 for temperature profiles and 0.83 for relative humidity profiles are obtained between the two data. Fig. 1 shows that in case of the temperature profile, radiosonde and radiometer data have a good matching. However above 2 km there is a small bias between the two instruments. In case of humidity profiles, some biases have been observed at various heights. The relative humidity profiles from a radiometer show a wet bias up to about 5 km and a dry bias above it and similar results were also observed by other researchers (Chan, 2009; Xu et al., 2014). This wet bias might due to the occasional occurrence of an elevated, moist layer not measured by the radiosondes (Chan, 2009). Another possible reason might be the variable weather conditions generated due to water vapor

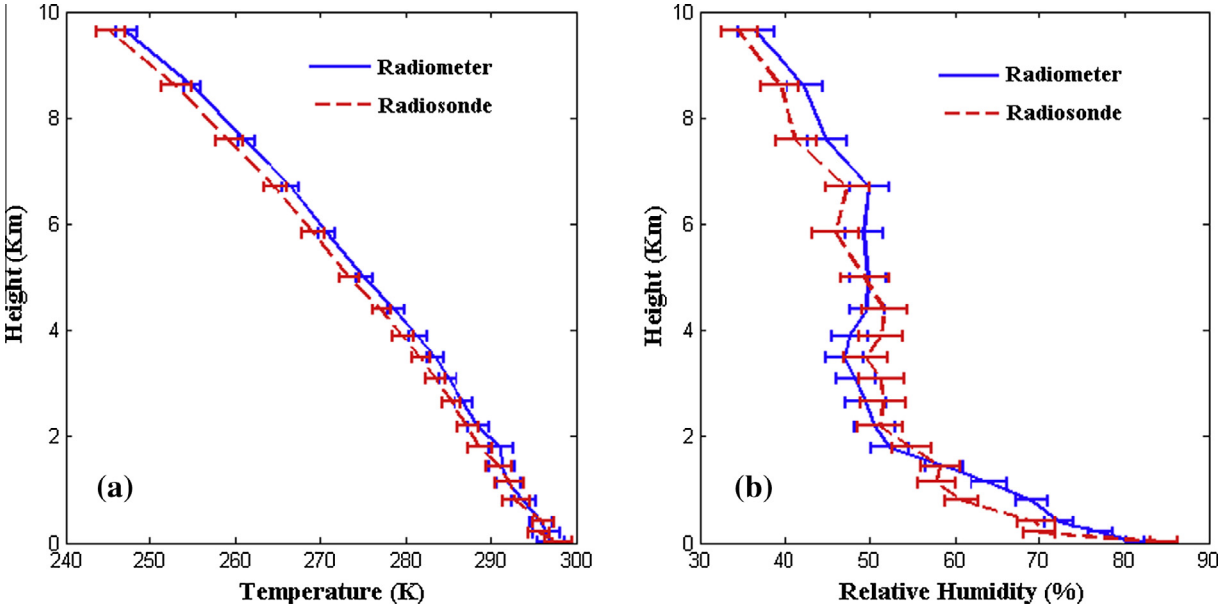

Fig. 1. Average profiles of parameters obtained from the radiosonde and radiometer (a) temperature and (b) relative humidity.

variability in the lower troposphere at the present location. This variability may not be detected by the inversion technique used by the radiometer utilizing the regression coefficients, obtained from a large number of radiosonde profiles which have an averaging effect. This comparison provides a quality check of our data in view of the fact that there are some inherent differences between the radiometric and radiosonde measurements as they involve two different techniques, have different vertical resolutions and are not co-located.

Currently, radiometric data for three years, from 2011 to 2013, are available, out of which one year data are used for developing the model and the rest of the data are used for validation which yielded a reasonably good performance of the proposed technique.

3. Methodology

During the developing stage of convection, the warm air rises up causing an updraft. The entrainment of warm air causes cold air from the surroundings to fill the region, thereby producing a cooling effect. This stage occurs before rain occurrence and it usually lasts for about 10–15 min (Byers and Braham, 1948; Rogers and Yau, 1982). Also, during the mature stage, a liquid mass, too heavy to be sustained as cloud, comes down in the form of rain generating precipitation drag and evaporative cooling and, thereby, producing a downdraft which cools the surface (Wakimoto, 1982).

To investigate this phenomenon, the temperature and humidity profiles are studied for some heavy rain events. It is observed that temperature decreases and humidity increases before rain events. The temperature and humidity profiles for a heavy rain event on 4 April 2011 are depicted in Fig. 2. For this event, the profiles have been analyzed from 1 h before rain to 1 h after the start of the rain event. Sharp changes in the profiles are observed about 20 min before the rain event starts.

The brightness temperatures in the water vapor absorption band (22–31 GHz) is used for humidity sensing in radiometer (Won et al., 2009). The absorption band for oxygen is at 58–60 GHz which is used for temperature sensing owing to the highly stable oxygen content in the atmosphere (Ullaby et al., 1982). As the temperature decreases and the humidity increases before rain, it is expected that changes in magnitude of brightness temperatures at these frequency bands will also occur before the rain events. The rain event on 4 April 2011 has been examined to trace the changes in the BT at 22 GHz and 58 GHz before rain (Fig. 3). Fig. 3 shows that the brightness temperature at 58 GHz decreases and the brightness temperature at 22 GHz increases at about 20 min before the start of heavy rain as expected. The rain rate variation during the day is shown in Fig. 3(b).

It is essential to check whether the changes in BT values at 22 GHz and 58 GHz before rain are significantly sharp and caused by definite changes in atmospheric parameters. For this reason, a set of 95 non-rainy days of 2011 and 2012 is selected. The non-rainy days refer to those days which do not experience rain at all. The next step is to find out the time interval during which most of the rain has occurred. It is seen from the frequency distribution that the maximum number of rain events start during 16:00–20:00 h (10:30–14:30 UTC). Hence, half hourly average variations of BT at 22 and 58 GHz from 9:00–14:00 UTC on non-rainy days are plotted in Fig. 4. It can be seen from the figure that there are no sharp changes in BT at the two frequencies during non-rainy days.

To check the variation of BT before rain, they are examined for 44 heavy rain events of 2011. The brightness temperature value at the start of rain event is kept as a reference to calculate the average variation of BT at various times before the rain. The average time-varying response of the BT before rain is shown in Fig. 5.

From Fig. 5, it can be seen that the BT of 22 GHz and 58 GHz show definite changes before rain. So these two BTs are used together to nowcast rain. But it is difficult to set any threshold to

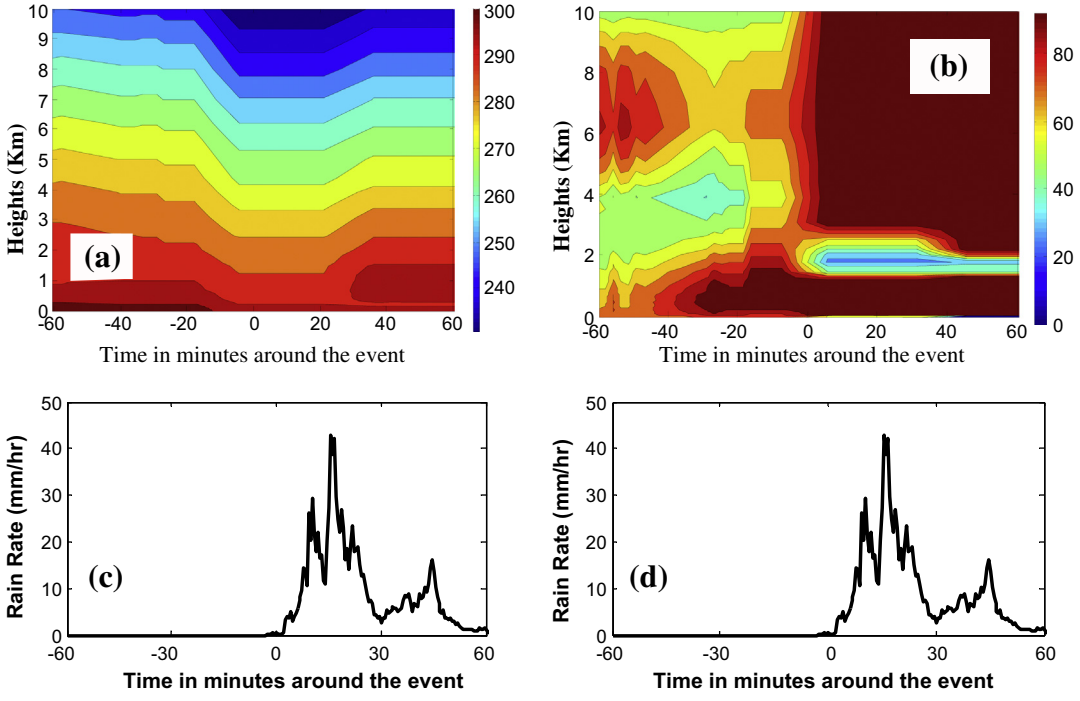

Fig. 2. Variation during a rain event of 4 April 2011 of the parameters: (a) temperature (K) at different heights, (b) humidity (%) at different heights, (c) and (d) rain rates during the event.

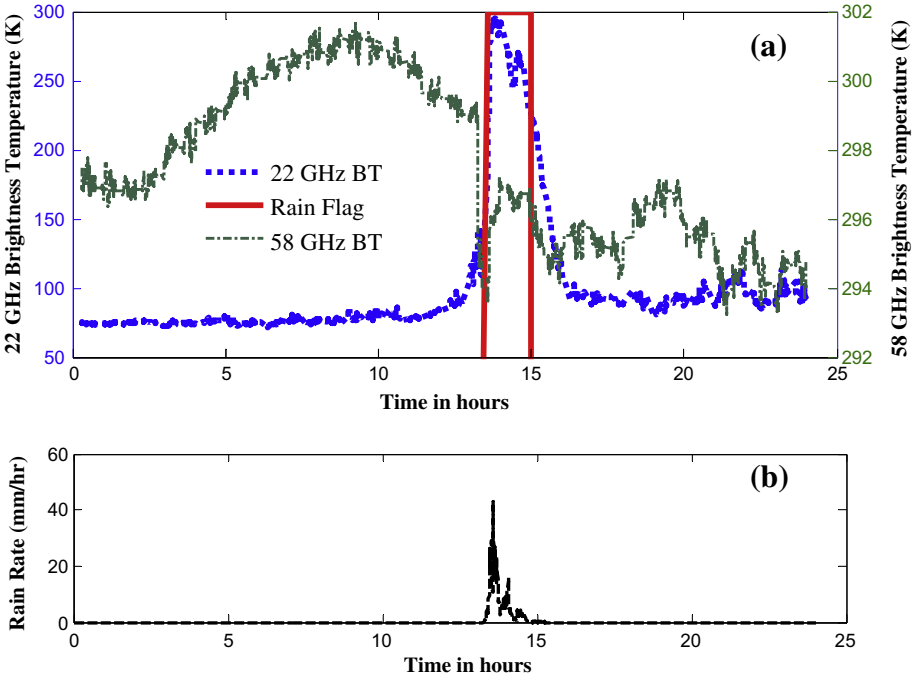

Fig. 3. Diurnal variation of parameters on 4 April 2011: (a) brightness temperatures at 22 GHz and 58 GHz and (b) rain rate variations during the day.

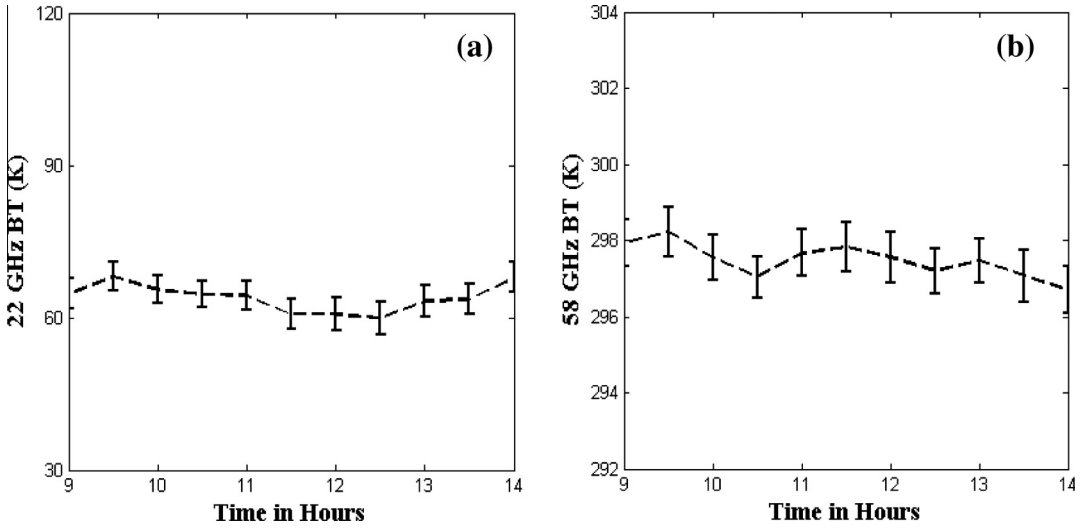

Fig. 4. Variation of BT for 95 non-rainy days: (a) brightness temperatures at 22 GHz and 58 GHz and (b) brightness temperatures at 58 GHz.

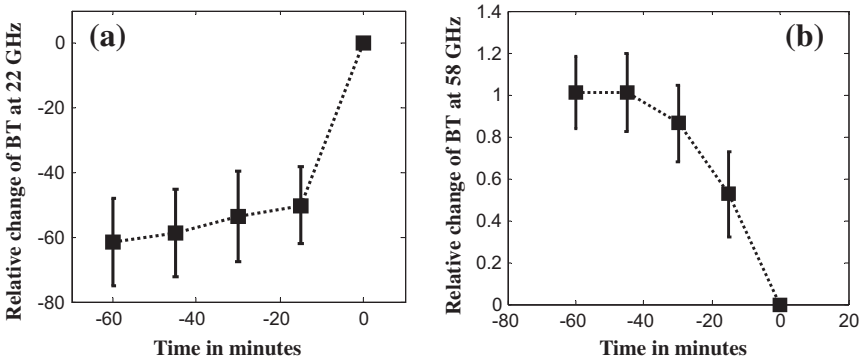

Fig. 5. Variation of brightness temperatures at (a) 22 GHz and (b) 58 GHz.

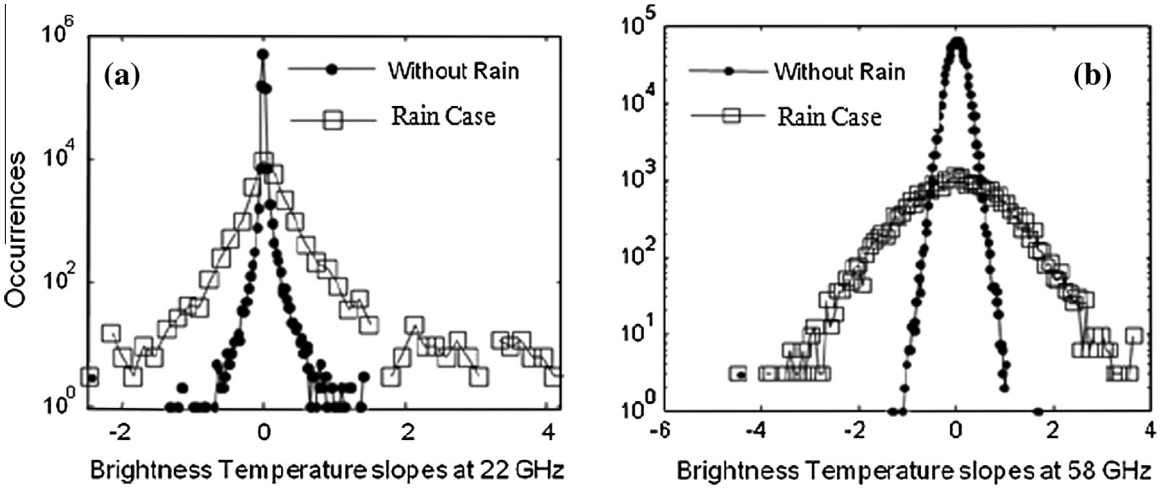

Fig. 6. Frequency distribution of brightness temperature slope of (a) 22 GHz and (b) 58 GHz.

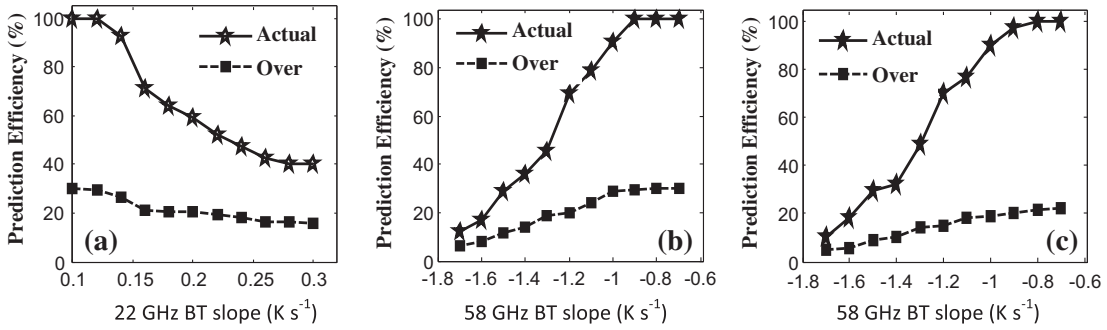

Fig. 7. Prediction efficiencies using (a) 22 GHz BT slope alone, (b) using 58 GHz BT slope alone and (c) using BT slopes at 22 GHz and 58 GHz.

these BT values as an indicator of rain as they suffer from diurnal and seasonal variability (Das et al., 2012). The first order time derivatives (slopes) of brightness temperatures of 22 and 58 GHz are therefore obtained with a time interval of 3 s.

A set of 44 rainy days is considered for developing the model. Since the technique generates an alarm periodically after 1 h, so a total of 44 × 24 h of observation have been considered segmenting it into one-hour periods. A one-hour period is considered as a wet period if rain has occurred during that hour, and if no rain is observed then the period is taken as a dry period.

The frequency distributions of the BT slopes are shown in Fig. 6 which shows that the spread of the distributions is larger in rain events than in absence of rain. The reason for this is that before rain, BT at 22 GHz shows a sharp increase due to increased moisture which is manifested by a large BT slope. Simultaneously, BT at 58 GHz decreases due to a cooling effect before convection as already explained, which results in a large slope as shown in the figure.

An algorithm in Matlab programming based on statistical data analysis is developed using the two BT slopes to nowcast rain. In the proposed technique, a sliding window of 1 h is used in which the values of brightness temperature slopes at 22 and 58 GHz are checked. An alarm is generated if both of these BT slopes exceed a certain threshold. Suitable threshold values for brightness temperature slopes have been obtained using two performance parameters. First one is the actual prediction efficiency defined as the percentage of rain events successfully predicted by the system. The second one is over prediction percentage giving the percentage

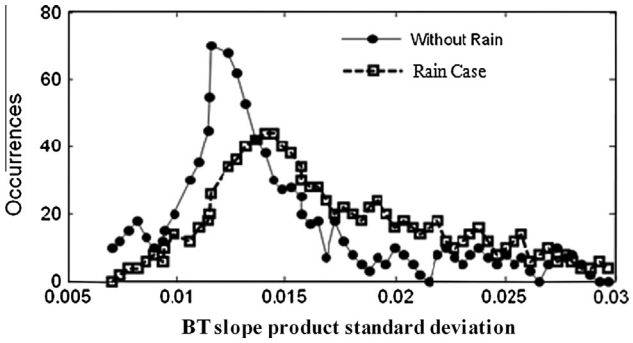

Fig. 8. Frequency distribution of standard deviation of brightness temperature slope product for rainy and dry instants.

of non-rain events for which false alarm is generated. Whenever the technique generates an alarm and rain occurs within the next one hour, then it is considered as a success. Number of events successfully predicted divided by the total number of rain events gives the actual prediction efficiency. However when an alarm is generated but rain has not occurred within next one hour then it is a false alarm. The number of false alarms divided by the number of no rain conditions give the over prediction rate. The threshold of rain prediction is considered as optimum if the actual prediction efficiency is greater than 90% and over prediction is as low as possible.

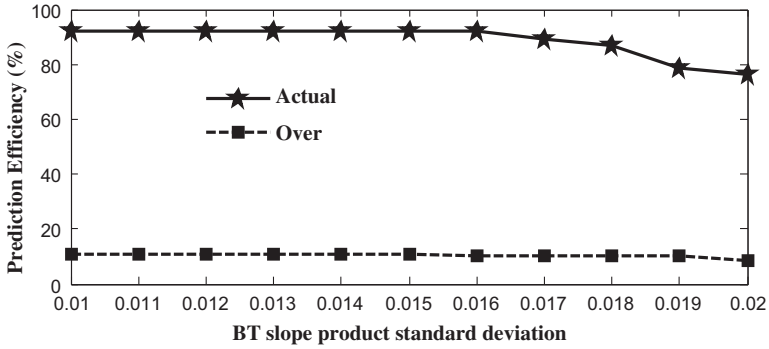

Fig. 9. Prediction efficiencies using BT slopes at 22 GHz and 58 GHz along with their product standard deviation.

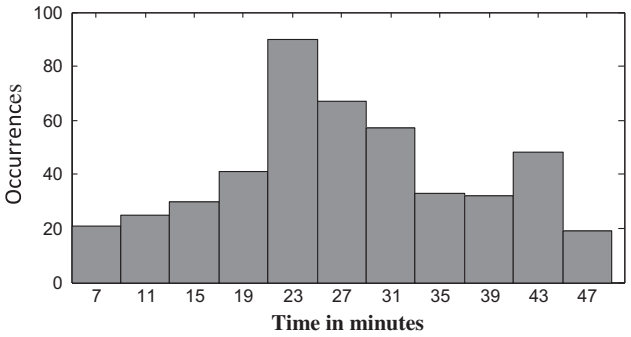

Fig. 10. Frequency distribution of time gap between alarm generation and rain event.

The prediction efficiency and false alarm rate are calculated for the BT slopes of 22 GHz. It has been seen that when the brightness temperature slope at 22 GHz before rain is 0.142 K s^{-1} the actual prediction is >90%, with 26% over prediction rate as shown in Fig. 7(a). When the same method is applied on slope of BT at 58 GHz, the prediction efficiency is greater than 90% at the slope value of −1 K s^{-1}, with an over prediction rate of 28% (Fig. 7(b)). Next, the above mentioned BT slopes at 22 GHz and 58 GHz are simultaneously considered. The slope of BT at 22 GHz is kept constant at 0.142 K s^{-1} while the slope of 58 GHz is varied. It is found that the prediction efficiency is 90% with a reduction in over prediction to 19% (Fig. 7(c)).

From the previous section it can be inferred that an optimum prediction efficiency of 90% has been obtained but the false alarm rate is still high. So the product of the slopes is considered to reduce the over prediction. As this parameter shows rapid fluctuations, the standard deviation of this product has been considered which determines whether the trend variation is due to a random phenomenon or due to a definite change in the slopes.

The frequency distribution of the standard deviation of BT slope product is shown in Fig. 8 which reveals that the spread of the

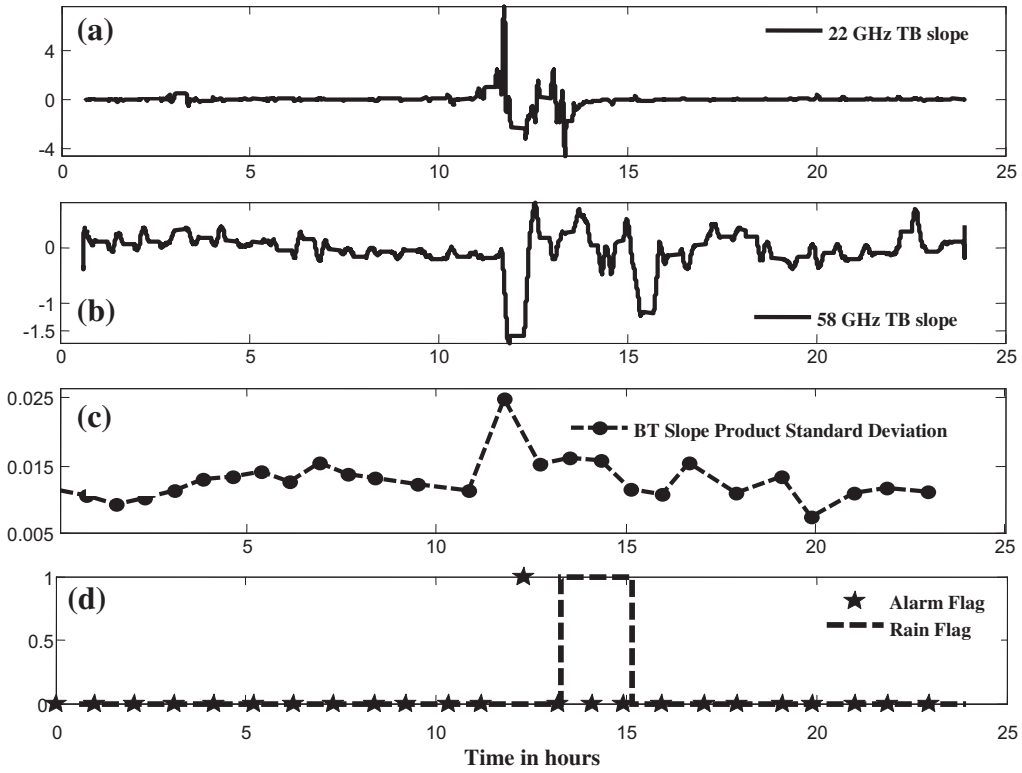

Fig. 11. Results obtained on 10 April, 2012 (a) brightness temperature slope at 22 GHz, (b) brightness temperature slope at 58 GHz, (c) brightness temperature slope product and (d) alarm and rain flag.

standard deviation is larger in rain cases than that without rain. As indicated in Fig. 6, the slopes of BT at 22 and 58 GHz are larger in rain cases than in the absence of rain. So, the product of the two slopes also increases causing a larger value of the standard deviation of this product. The range of BT slope product standard deviation is 0.01–0.03 $K^2 s^{-2}$ before rain events which is included in the algorithm. The value of standard deviation of the BT slope product is checked over a sliding window of 8 h. However, the last one hour of the window is used for checking the brightness temperature slopes at 22 and 58 GHz. The BT slopes of 22 GHz and 58 GHz are kept fixed at 0.142 $K s^{-1}$ and -1 $K s^{-1}$ respectively as shown in Fig. 7(a) and (b) and the prediction efficiencies are checked for different values of the standard deviation of BT slope product. It is seen that when the standard deviation threshold is 0.016 $K^2 s^{-2}$, the actual prediction efficiency is 92% while the over prediction percentage has reduced to 10% which can be considered to be within reasonable limit shown in Fig. 9.

4. Validation

To validate the efficacy of the model, it is tested on a new dataset comprising 130 rainy days of premonsoon and monsoon period of 2012 (March 2012–September 2012) and premonsoon season of 2013 (March 2013–June 2013). The actual prediction efficiency obtained is about 90% while the over prediction is 11%.

The time difference between event occurrences and alarm generation is recorded for all events. When the frequency distribution of these time gaps is plotted, it is seen that the alarm is mostly generated around 25 min before the rain events as shown in Fig. 10.

Fig. 11 shows a random rain event on 10 April, 2012. In Fig. 11(a) and (b), the BT slopes at 22 and 58 GHz are shown, respectively. The variations of the standard deviation of the slope products are shown in Fig. 11(c). Large fluctuations are seen on both the slopes with high standard deviation value. The proposed model has thus generated an alarm about 40 min before the rain as indicated in Fig. 11(d).

5. Conclusions

In this paper it has been observed that the brightness temperature at 22 and 58 GHz, which are sensitive to humidity and temperature profiles respectively, have shown sharp changes before rain. So, the simultaneous variations of brightness temperatures at 22 and 58 GHz have been utilized to nowcast heavy precipitations. The present technique involves radiometric observations in the water vapor as well as the oxygen absorption band which has not yet been reported in open literature. A model has been developed using the first order derivatives of brightness temperatures at 22 and 58 GHz and the standard deviation of their product. The procedure gives a good nowcasting capability when tested for a number of rain events in 2012–2013. The proposed technique provides a prediction efficiency of 90% with a false alarm rate of 10% which is better compared to other traditional methods of nowcasting. The most of the alarms are generated about 25 min prior to rain events indicating that it can be a useful tool to predict rain occurrences. This technique is less involved and provides continuous prediction. The present technique cannot predict the rain intensity as it utilizes only brightness temperature gradients. However, with the incorporation of some additional parameters such as, liquid water content and integrated water vapor, the present technique might be upgraded to forecast rain intensity which can be a subject matter of a future investigation. Since the present technique provides continuous and more efficient prediction, it can be useful for aviation and defense applications. It should also be noted that the present technique is based on physical reasoning related to atmospheric processes before rain and is expected to work in other locations as well, particularly with similar climatic conditions.

Acknowledgement

The financial support provided by Indian Space Research Organisation (ISRO), India under the projects (1) "Integrated studies on water vapor Liquid Water content and Rain of Tropospheric atmosphere and effects in Radio Environment" and (2) "Space Science Promotion Scheme" are thankfully acknowledged.

References

Browning, A.K., 1982. A Very Short Range Forecasting of Precipitation by the Objective Extrapolation of Radar and Satellite Data in Nowcasting. Academic Press, U.S.A, 177.

Byers, H.R., Braham Jr., R.R., 1948. Thunderstorm structure and circulation. J. Atmos. Sci. 5 (3), 71–86.

Chan, P.W., 2009. Performance and application of a multi-wavelength, ground-based microwave radiometer in intense convective weather. Meteorologische Zeiteschrift 18 (3), 253–265.

Chan, P.W., Lee, Y.F., 2011. Application of ground based multi-channel microwave radiometer to the alerting low level wind shear. Meteorologische Zeiteschrift 20 (4), 423–429.

Cluckie, I.D., Collier, C.G., 1991. The combined use of weather radar and mesoscale numerical model data for short-period rainfall forecasting, In: Cluckie I.D. Collier C.G. (Eds.), Hydrological Applications of Weather Radar. E. Horwood (Ellis Horwood Series In Environmental Management, Science, And Technology), New York, pp. 331–348.

Darkow, G.L., 1968. The total energy environment of severe storms. J. Appl. Meteorol. 7 (2), 199–205.

Das, S., Chakraborty, R., Talukdar, S., Maitra, A., 2012. Nowcasting of tropical rain using dual frequency atmospheric brightness temperatures at Kolkata. In: 2012 5th International Conference on Computers and Devices for, Communication (CODEC), vol. 1(4). pp. 17–19. http://dx.doi.org/10.1109/CODEC.2012.6509338.

Dutta, D., Sarma, D.K., Kumar, M., Sharma, S., Vishwanathan, G., Gairola, R.M., Das, J., Kannan, B.A.M., Venkateswaralu, S., 2010. Nowcasting of yes/no situation at a station using soft computing technique to the radar imagery. IJRSP 39, 92–102.

Dvorak, P., Mazanek, M., Zvanovec, S., 2012. Short-term prediction and detection of dynamic atmospheric phenomena by microwave radiometer. Radioengineering 21 (4), 1060–1066.

Faubush, E.J., Miller, R.C., Starrett, L.G., 1951. An empirical method for forecasting tornado development. Bull. Am. Meteorol. Soc. 32, 19.

Galway, J.G., 1956. The lifted index as a predictor of latent instability. Bull. Am. Meteorol. Soc. 37, 528–529.

Geerts, B., 2001. Estimating downburst related maximum surface wind speeds by means of proximity soundings in New South Wales, Australia. Weather Forecast. 16, 261–269.

Güldner, J., Spänkuch, D., 1999. Result of year round remotely sensed integrated water vapor by ground based microwave radiometry. J. Appl. Meteorol. 38, 981–988.

Johnson, L.E., Olsen, B.G., 1998. Assessment of quantitative precipitation forecasts. Weather Forecast. 13, 75–83.

Koffi, E.N., Schneebeli, M., Brocard E., Mätzler, C., 2007. The Use of Radiometer Derived Convective Indices in Thunderstorm Nowcasting, Mätzler Research Report Nr. 2007-02-MW March 2007 Bern University.

Lin, C., Vasić, S., Kilambi, A., Turner, B., Zawadzki, I., 2005. Precipitation forecast skill of numerical weather prediction models and radar nowcasts. Geophys. Res. Lett. 32, L14801.

Madhulatha, A., Rajeevan, M., Venkat Ratnam, M., Bahte, J., Naidu, C.V., 2013. Nowcasting severe convective activity over southeast India using ground based microwave radiometer observations. J. Geophys. Res. 118, 1–13.

Manzato, A., 2003. A climatology of instability indices derived from Friuli Venezeilia Giulia soundings using three different methods. Atmos. Res. 67–68, 417–454.

McCann, D.W., 1994. WINDEX – a new index for forecasting microburst potential. Weather Forecast. 9, 532–541.

Mecklenburg, S., Joss, J., Schmid, W., 2000. Improving the nowcasting of precipitation in an Alpine region with an enhanced radar echo tracking algorithm. J. Hydrol. 239, 46–68.

Rogers, R.R., Yau, M.K., 1982. A Short Course in Cloud Physics, third ed. (International Series in Natural Philosophy), Canada, p. 222.

Rose, Th., Czekala, H., 2009. RPG-HATPRO Radiometer Operating Manual, Radiometer Physics GmbH, Version 7.99.

Sherwood, S.C., Roca, R., Weckwerth, T.M., Andronova, N.G., 2010. Tropospheric water vapor, convection, and climate. Rev. Geophys. 48 (2), RG2001.

Showalter, A.K., 1953. Stability index for forecasting thunderstorms. Bull. Am. Meteorol. Soc. 34, 250–252.

Sokol, Z., 2006. Nowcasting of 1-h precipitation using radar and NWP data. J. Hydrol. 328, 200–211.

Ullaby, F.T., Moore, R.K., Fung, A.K., 1982. Microwave remote sensing: active and passive. Volume Scattering and Emission Theory, Advanced Systems and Applications, vol. III. Artech House, Inc., Dedham, Massachusetts.

Wakimoto, R.M., 1982. The life cycle of thunderstorm gust fronts as viewed with doppler radar and radiosonde data. Monthly Weather Rev. 110, 1060–1082.

Wang, P., Smeaton, A., Lao, S., O'Connor, E., Ling, Y., O'Connor, N., 2009. Short-Term Rainfall Nowcasting: Using Rainfall Radar Imaging Eurographics Ireland.

Wilson, J.W., Crook, A.N., Mueller, C.K., Sun, J., Dixon, M., 1998. Nowcasting thunderstorms: a status report. Bull. Am. Meteorol. Soc. 79, 2079–2099.

Won, H.Y., Kim, Y.H., Hee-Sang, 2009. Application of brightness temperature received from ground-based microwave radiometer to estimation of precipitation occurrences and rainfall intensity. Asia Pacific J. Atmos. Sci. 45, 55–69.

Xu, G., Randolph, W., Zhang, W., Feng, G., Liao, K., Liu, Y., 2014. Effect of off-zenith observations on reducing the impact of precipitation on ground-based microwave radiometer measurement accuracy. Atmos. Res. 140–141, 85–94.

Zahraei, A., Kuo-lin, H., Sorooshian, S., Gourley, J.J., Hong, Y., Behrangi, A., 2013. Short-term quantitative precipitation forecasting using an object-based approach. J. Hydrol. 483, 1–15.